Cu metal embedded in oxidized matrix catalyst to promote CO_2 activation and CO dimerization for electrochemical reduction of CO_2

Hai Xiao[a], William A. Goddard III[a,1], Tao Cheng[a], and Yuanyue Liu[a,b]

[a]Materials and Process Simulation Center and Joint Center for Artificial Photosynthesis, California Institute of Technology, Pasadena, CA 91125; and [b]The Resnick Sustainability Institute, California Institute of Technology, Pasadena, CA 91125

Contributed by William A. Goddard III, May 9, 2017 (sent for review February 13, 2017; reviewed by Timo Jacob and Bruce Parkinson)

We propose and validate with quantum mechanics methods a unique catalyst for electrochemical reduction of CO_2 (CO_2RR) in which selectivity and activity of CO and C_2 products are both enhanced at the borders of oxidized and metallic surface regions. This Cu metal embedded in oxidized matrix (MEOM) catalyst is consistent with observations that Cu_2O-based electrodes improve performance. However, we show that a fully oxidized matrix (FOM) model would not explain the experimentally observed performance boost, and we show that the FOM is not stable under CO_2 reduction conditions. This electrostatic tension between the Cu^+ and Cu^0 surface sites responsible for the MEOM mechanism suggests a unique strategy for designing more efficient and selective electrocatalysts for CO_2RR to valuable chemicals (HCO_x), a critical need for practical environmental and energy applications.

electrochemical reduction of CO_2 | Cu metal embedded in oxidized matrix | density functional theory | CO_2 activation | CO dimerization

Electrochemical reduction of CO_2 (CO_2RR) to valuable chemicals is an essential strategy to achieve industrial-scale reduction of the carbon footprint under mild conditions and to provide a means of storing electrical power from intermittent renewable sources into stable chemical forms (1). Cu is the prototype electrocatalyst for CO_2RR, because it is the only pure metal that delivers appreciable amounts of methane and ethylene plus minor alcohol products (2–7), but it suffers from high overpotentials and very significant hydrogen evolution reactions (HERs). Consequently, tremendous efforts are being made to develop more efficient and selective electrocatalysts, for example by surface modification (8) and by nanoparticle (9, 10) and nanowire (11) engineering.

We examine here the mechanism by which Cu_2O-based electrodes are observed to improve both efficiency and selectivity for C_2 products (12–15), which also suppresses HERs by several-fold. Because Cu_2O is subject to reduction (back to Cu metal) under CO_2RR conditions, the improved performance was initially attributed to Cu metal surface morphology (8, 16). But a more recent experiment (15) showed that Cu^+ sites can survive on the Cu surface for the course of CO_2RR. Importantly, a Cu sample that is first oxidized and then reduced using an H2 plasma leads to performance substantially worse than that of the oxidized sample, despite both having similarly roughened surfaces. This provides solid evidence that surface Cu^+ plays an essential role in promoting the efficiency and selectivity of CO_2RR. However, experiments have provided no clue about how surface Cu^+ affects the mechanisms of CO_2RR. Moreover, no previous theoretical efforts have elucidated its role.

To understand the promising results achieved with Cu_2O-based electrodes, we investigated three distinct models aimed at unraveling the role of surface Cu^+ in shaping the free energy profiles of two key steps for CO_2RR. Here we carry out quantum mechanics (QM) calculations at constant potential by using our grand canonical methodology (17, 18) that uses the charge-asymmetric nonlocally determined local-electric (CANDLE) implicit solvation model (19) to achieve constant electrochemical potential (not constant number of electrons) within the framework of joint density functional theory (JDFT) (20, 21) (details in *Computational Details*). The three key steps we focus on are (*i*) CO_2 activation, which we previously showed to be the rate-determining step (RDS) for CO production on pure Cu (22); (*ii*) CO dimerization, which we previously showed to be the RDS for forming C_2 products from CO on pure Cu (17, 18); and (*iii*) C_1 product formation, which we find to compete with C_2 products for pure Cu.

We find that the surface Cu^+ by itself actually deteriorates the performance of CO_2RR. Instead we show that it is synergy between surface Cu^+ and surface Cu^0 that improves significantly the kinetics and thermodynamics of both CO_2 activation and CO dimerization, while making C_1 unfavorable, thereby boosting the efficiency and selectivity of CO_2RR. These results provide a unique concept for designing improved electrocatalysts. To illustrate this synergy we consider the case with an applied potential U = −0.9 V [referenced to standard hydrogen electrode (SHE)], which is where CO production reaches the peak and C_2 production begins on the oxide electrode (15). The free energies at any other U can be calculated using Table S1.

Fig. 1 shows the three surface models we used to probe the role of surface Cu^+ in CO_2RR. Fig. 1*A* shows the metallic matrix (MM), where the pristine Cu(111) surface serves as a reference model for pure MM that has only Cu^0 on the surface Fig. 1*B* shows the fully oxidized matrix (FOM), where the stoichiometric nonpolar Cu_2O(111) surface serves as a model for a FOM with only Cu^+ on the surface. Here we find two types of Cu^+ surface

Significance

A most promising approach to boosting both efficiency and selectivity for electrochemical reduction of CO_2 (CO_2RR) is using Cu_2O-based electrodes, and the surface Cu^+ is believed to play an essential role that is totally unclear from both experiment and theory. We find that the surface Cu^+ by itself actually deteriorates the performance of CO_2RR. Instead we propose a Cu metal embedded in oxidized matrix (MEOM) model and show that it is synergy between surface Cu^+ and surface Cu^0 present in the MEOM model that improves significantly the kinetics and thermodynamics of both CO_2 activation and CO dimerization, thereby boosting the efficiency and selectivity of CO_2RR. The MEOM model serves as a unique platform for design of better electrocatalysts for CO_2RR.

Author contributions: H.X. and W.A.G. designed research; H.X. and T.C. performed research; H.X., W.A.G., T.C., and Y.L. analyzed data; and H.X. and W.A.G. wrote the paper.

Reviewers: T.J., Universität Ulm; and B.P., University of Wyoming.

The authors declare no conflict of interest.

Freely available online through the PNAS open access option.

[1]To whom correspondence should be addressed. Email: wag@wag.caltech.edu.

This article contains supporting information online at www.pnas.org/lookup/suppl/doi:10.1073/pnas.1702405114/-/DCSupplemental.

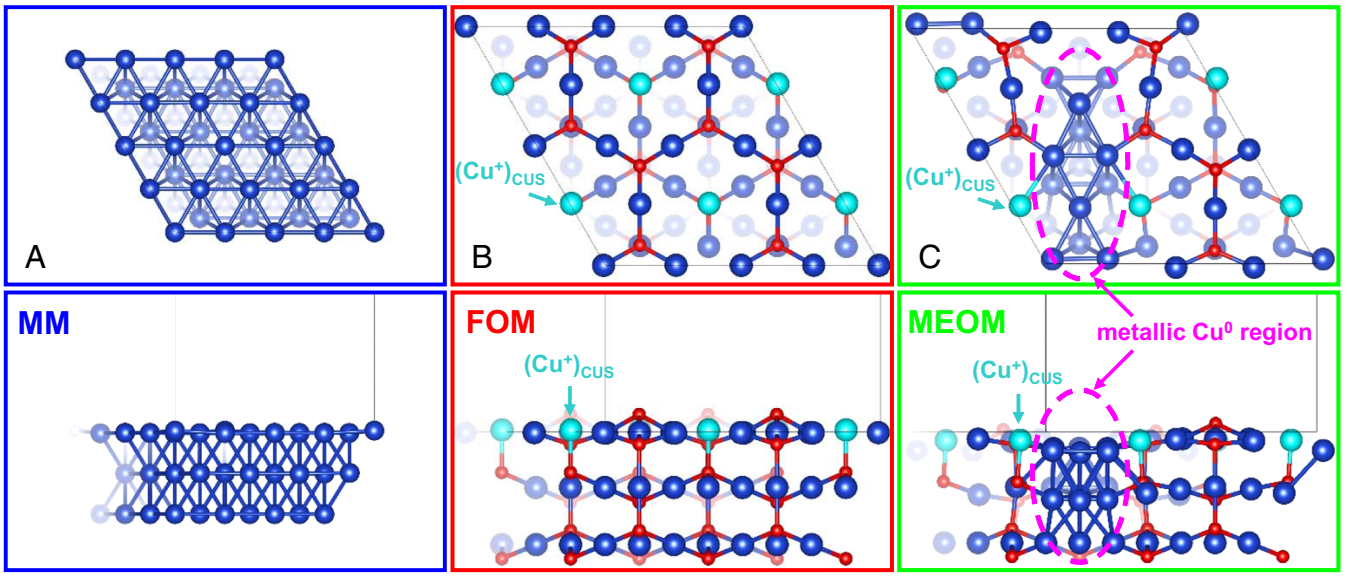

Fig. 1. Top and side views of the three surface models. (*A*) A 4 × 4 Cu(111) surface, the model for a metallic matrix (MM). (*B*) A 2 × 2 Cu_2O(111) surface, the model for fully oxidized matrix (FOM). (*C*) Metal embedded in oxidized matrix (MEOM) derived by reducing one-quarter of a 2 × 2 Cu_2O(111) surface. Here Cu is dark blue, with the active $(Cu^+)_{CUS}$ marked light blue, and red is O. Purple dashes mark the border between Cu^0 and Cu^+ regions. (Please refer to Fig. S7 for Bader charge analysis of surface Cu sites on FOM and MEOM models.)

sites: $(Cu^+)_{CSS}$, a coordinatively saturated Cu^+ site that is bonded to two O atoms, and $(Cu^+)_{CUS}$, a coordinatively unsaturated site that is bonded to only the one O atom directly below it (examples are marked in Fig. 1*B*). The $(Cu^+)_{CUS}$ is believed to be the active site (ref. 23 and references therein). However, it has been suggested by both theory (24) and experiment (25) that such $(Cu^+)_{CUS}$ sites are likely missing under oxygen-rich conditions (e.g., oxygen plasma treatment). More recent theoretical work (26) has shown that $(Cu^+)_{CUS}$ sites are favored under CO_2RR conditions at neutral pH. Here we focus on the role of active surface Cu^+ in shaping the energetics and mechanisms of CO_2RR, rather than stability. Fig. 1*C* shows metal embedded in oxidized matrix (MEOM), a partially reduced Cu_2O(111) surface in which one-quarter of the surface is reduced. This serves as a conceptual model for our MEOM in which both Cu^0 and Cu^+ are present on the surface. We find that this leads to active $(Cu^+)_{CUS}$ sites at the edge of metallic Cu^0 regions that play an essential role in the enhanced activity. Our MEOM catalyst site mimics the case for CO_2RR operation, where the majority of surface stays oxidized but some reduced regions are created.

We focus here on the (111) surface orientation, because it is the most stable among Cu_2O surfaces (27) and has the fastest kinetics for Cu surface oxidation (28) (thus the most likely oxide surface orientation from oxidation of Cu foil). In the experiment that directly compared the metal with oxide surfaces (15), the measured onset potentials for C_2H4 production on Cu metal surfaces are −1.2 V to −1.1 V (this is the value for both electropolished and roughened surfaces obtained by first oxidizing and then reducing the Cu foil with hydrogen plasma), which are the same as the onset potentials measured on a Cu(111) single crystal electrode (−1.2 V to −1.1 V), but very different from the value of −0.8 V to −0.6 V measured on Cu(100) (29, 30).

CO_2 Activation

MM Model. We find that physisorption of CO_2 ($CO_{2,phys}$) on the MM model leads to a noncovalent bond distance of 3.84 Å between the C atom of linear CO_2 and the Cu surface (C-Cu_s; Fig. S1*A*), which is similar to our previous study (22). Forming chemisorbed bent CO_2 ($CO_{2,chem}$) from this $CO_{2,phys}$ involves a transition state (TS) that bends CO_2 with C-Cu_s = 2.36 Å, and the resulting $CO_{2,chem}$ is asymmetrically adsorbed, with a surface CuO = 2.04 Å, whereas the second O atom pointing away from the surface to form a hydrogen bond (1.52 Å) to a surface H_2O bonded to a nearby Cu^0 (Fig. S1*C* and Fig. 2). On the MM model the activation free energy barrier is $\Delta G^{\neq}$ = 0.49 eV at 298 K, similar to the value (0.43 eV) for Cu(100) in our previous study (22).

FOM Model. It was proposed (23) that in the FOM model CO_2 can adsorb at the $(Cu^+)_{CUS}$ site with a 2.09-Å bond of one O to $(Cu^+)_{CUS}$. However, exposed to the electrolyte, the $(Cu^+)_{CUS}$ sites are mostly occupied by H_2O molecules [strong electronic binding energy of $\Delta E = -0.98$ eV, much larger than that for CO_2 ($\Delta E = -0.31$ eV)]. Thus, the initial structure for CO_2 activation on the FOM model is still physisorption of CO_2 with a 4.07-Å distance between the C atom of linear CO_2 and O_s, the closest surface O atom (Fig. S2*A*). We find a $\Delta G^{\neq}$ = 0.56 eV to convert this $CO_{2,phys}$ to a surface carbonate (Fig. 2), which can subsequently be released into the electrolyte, thereby reducing

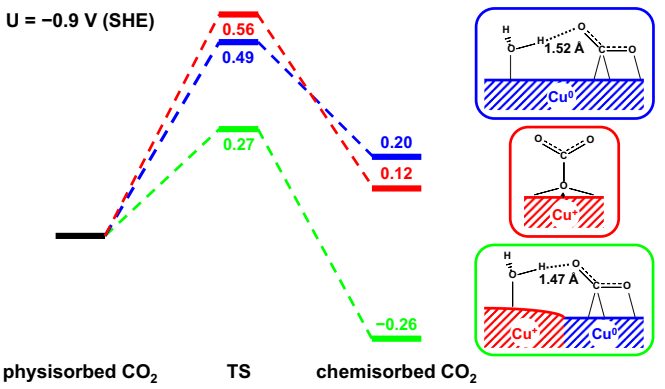

Fig. 2. Free energy profiles (at U = −0.9 V) for CO_2 activation on the MM (blue), FOM (red), and MEOM (green) models, including the resulting chemisorbed CO_2 structures. Note that FOM leads to a surface carbonate product.

the FOM surface. Therefore, CO_2 activation in the FOM model has a barrier 0.07 eV higher than the MM model and involves a different mechanism that does not lead to the key intermediate (chemisorbed CO_2) for CO production. This indicates that the experimentally observed promotion of CO production using oxidized electrodes (12, 13, 15) cannot be explained with the presence only of surface Cu^+.

MEOM Catalyst. In contrast, the MEOM surface has a metallic Cu^0 region bordered by the Cu^+ oxide matrix. Here physisorbed CO_2 is favored on top of the Cu^0 region (Fig. S3*A*), and the activation of CO_2 proceeds through a TS that bends CO_2 just as in the MM case (Fig. S3*B*), leading to the asymmetrically chemisorbed CO_2 on the Cu^0 region. But now the free energy barrier is $\Delta G^{\neq} = 0.27$ eV, which is 0.22 eV lower than for the MM model. Moreover, the chemisorbed CO_2 is $\Delta G = -0.26$ eV more stable than physisorbed CO_2 on the MEOM catalyst (Fig. 2).

This drastic improvement in both kinetics and thermodynamics for the MEOM catalyst is due to the presence of $(Cu^+)_{CUS}$ sites that bind H_2O molecules at the edge of the Cu^0 region. This H_2O molecule on the $(Cu^+)_{CUS}$ site forms strong hydrogen bonds to the CO_2, stabilizing both the TS and the final state (FS) (Fig. 2). This opens a channel in which the negative charge accumulated on the O atom of the CO_2 during activation is distributed to the Cu^+ region, thus stabilizing both the TS and the FS.

Summarizing, only this MEOM catalyst with both surface Cu^0 regions (binds to activated CO_2) and Cu^+ (dilutes negative charge) sites has the ability to enable promotion of CO_2 activation, with favorable kinetics and thermodynamics. This explains the experimental observation that both the onset potential and the peak Faradaic efficiency for CO production are improved for CO_2RR on oxide-based electrodes (12, 13, 15). We propose that our MEOM catalyst might also provide the mechanism by which partially oxidized atomic cobalt layers improve formate production (31).

CO Dimerization

MM Model. CO dimerization on the MM model has been thoroughly studied by us and others (17, 32). The initial structure of two well-separated adsorbed CO molecules (Fig. S4*A*) goes through a TS that tilts and draws the two COs close (Fig. S4*B*), with $\Delta G^{\neq} = 1.10$ eV, to form an OCCO surface species with a 1.52-Å C-C bond (Fig. S4*C*).

FOM Model. In contrast, CO dimerization in the FOM model takes a distinctly different path. A CO molecule introduced near the FOM surface (either direct or from CO_2RR) binds to the $(Cu^+)_{CUS}$ site by $\Delta E = -1.62$ eV, displacing the H_2O ($\Delta E = -0.98$ eV). Thus, CO dimerization starts with two strongly adsorbed CO molecules on neighboring $(Cu^+)_{CUS}$ sites (Fig. S5*A*), which proceeds through an asymmetric TS (Fig. S5*B*) that rotates both CO molecules to have O atoms bonded to the $(Cu^+)_{CUS}$ sites (initially C atoms were bonded) with the C atom of one CO molecule bonded to the $(Cu^+)_{CSS}$ site in between. The resulting OCCO surface species (Fig. S5*C* and Fig. 3) is formed with a C=C double bond (1.30 Å) with each C atom bonded to the middle $(Cu^+)_{CSS}$. This is the only stable CO dimer on the FOM surface, but the formation barrier is $\Delta G^{\neq} = 3.15$ eV, and the product has a free energy unstable by $\Delta G = 2.25$ eV. Thus, the presence of only Cu^+ at the active surface cannot explain the experimental observation that C_2 products are promoted with oxidation-treated electrodes (13–15).

MEOM Catalyst. On the MEOM surface, CO also adsorbs on the $(Cu^+)_{CUS}$ site ($CO@Cu^+$), more stable by 0.48 eV than on the metallic Cu^0 region ($CO@Cu^0$).With MEOM, CO dimerization from two neighboring $CO@Cu^+$ is the same in nature as that on the FOM surface, so it would lead to the same $\Delta G^{\neq}$ (3.15 eV) as for the FOM. However, CO dimerization starting with $CO@Cu^0$ and a neighboring $CO@Cu^+$ (Fig. S6*A*) has a modest barrier of $\Delta G^{\neq} = 0.71$ eV to form the OCCO surface species, in which the two C atoms are still bonded to the Cu^+ and Cu^0 regions (Fig. S6*C*), leading to $\Delta G = 0.12$ eV (Fig. 3). The favorable energetics of this C-C coupling can be understood by noting that the C atom of $CO@Cu^+$ is positively charged (Mulliken charge of +0.11) whereas the C atom of $CO@Cu^0$ is negatively charged (Mulliken charge of −0.31) due to back donation. Thus, the attractive electrostatics between the two Cs assists C-C bond formation. It is this favorable dimerization process on the MEOM model that improves both kinetics and thermodynamics of the RDS for C_2 products, compared with the traditional MM model (Fig. 3). Thus, we propose that promotion of C_2 products for oxidation-treated electrodes arises from the MEOM surface via the mechanism described above (13–15).

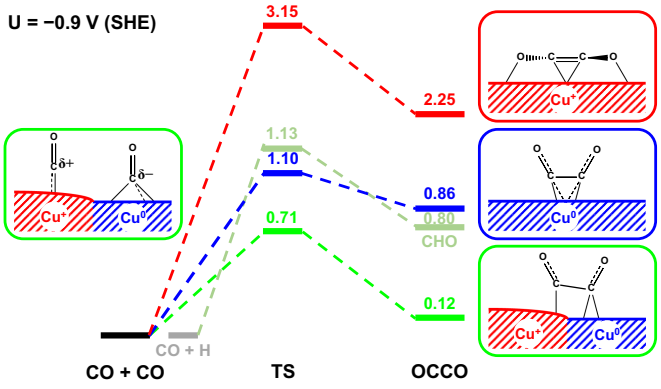

Fig. 3. Free energy profiles (at U = −0.9 V) of CO dimerization in the MM (blue), FOM (red), and MEOM (green) models and for CO hydrogenation to form surface CHO species in the MEOM model (gray green) at pH 7. *Right* shows resulting surface OCCO structures, whereas *Left* shows the initial structure on the MEOM model, which shows that the C atoms of the two COs on the Cu^+ and Cu^0 regions are positively and negatively charged, respectively, which assists the C-C coupling.

The major C_2 products from CO_2RR have been reported to be either ethylene (13, 15) or ethanol (14), where the major difference in these experiments is the pH (neutral pH for ethylene and basic pH for ethanol). We have shown recently (18) that the energetics of surface water determine the selectivity of alcohol vs. hydrocarbon products. We found that at neutral pH it is favorable for surface water to donate a proton for dehydroxylation to form hydrocarbon products. Whereas in basic pH the ability of surface water to dehydroxylate the surface species is suppressed (because the product OH− is less favorable), favoring instead the alcohol product (ethanol).

C_1 Pathways

Next we consider the possible pathways for forming C_1 with the MEOM surface. Here we expect $CO@Cu^+$ and $H@Cu^0$. Interestingly, the COH pathway previously proposed by us (17, 33) is an unreasonable option, because $COH@Cu^+$ is higher than $CHO@Cu^+$ by $\Delta G = 1.86$ eV. This also eliminates the CO-COH pathway for C_2 products we previously proposed (17). On the other hand, the CHO pathway has a reasonable free energy barrier of $\Delta G^{\neq} = 1.13$ eV (Fig. 3) at neutral pH, which is still significantly higher than the $\Delta G^{\neq} = 0.71$ eV for C-C coupling with $CO@Cu^+$ and $CO@Cu^0$. Consequently the stability of $CO@Cu^+$ (which is more resistant to hydrogenation) blocks the C_1 products. This selectivity for C_2 over C_1 is intrinsic and not due to the external local high-pH effect as speculated previously (13, 15).

Notes on the MEOM Catalyst

The MEOM concept is in fact a synergistic metal and oxidized matrix cocatalyst, with both ingredients directly participating in catalysis. Thus, for the MEOM model to be effective, it is necessary for the metal surface to be level with the oxidized matrix surface so that the surface species can interact via proper geometries. Therefore, a suitable scheme to generate the MEOM catalyst is deriving the metal directly from the oxidized matrix surface as in our construction of the MEOM model, which is also consistent with the current experimental strategy. This scheme can be naturally extended to starting with a mixed oxidized matrix (e.g., Cu_2O/Ag_2S) for alternative oxidized matrices.

Summary

We present the MEOM model for a partially oxidized Cu surface and show that this model leads to plausible mechanisms to explain the experimental findings that CO_2RR can be made more efficient and selective, using oxidized electrodes. However, MEOM requires that we only partially oxidize the surface. This MEOM model presents a unique guideline for design of improved CO_2RR electrocatalysts. In contrast to previous speculations, we find that the active surface Cu^+ sites alone do not improve the efficiencies of CO_2RR and indeed deteriorate the efficiency. Instead the synergy between active surface Cu^+ and Cu^0 regions present in the MEOM model is responsible for improving significantly the kinetics and thermodynamics of both CO_2 activation and CO dimerization while impeding C_1 pathways, the key steps for efficiency and selectivity of CO_2RR.

Based on our MEOM model, we conclude that the oxidized matrix (Cu_2O) is unstable under CO_2RR working conditions. We find that the role of the Cu_2O is mainly electrostatic in diluting the negative charge built up on the CO_2 as it transitions from physisorbed to chemisorbed structures, which in turn makes the C atom of CO positively charged. This MEOM model suggests alternative oxidized matrices (like Ag_2S) could also deliver similar electrostatic contributions, leading to much improved electrochemical stabilities.

ACKNOWLEDGMENTS. This research was supported by the Joint Center for Artificial Photosynthesis, a Department of Energy (DOE) Energy Innovation Hub, supported through the Office of Science of the US DOE under Award DE-SC0004993. This work used the computational resources of Zwicky (at California Institute of Technology).

1. Zhu DD, Liu JL, Qiao SZ (2016) Recent advances in inorganic heterogeneous electrocatalysts for reduction of carbon dioxide. *Adv Mater* 28:3423–3452.
2. Hori Y, Kikuchi K, Suzuki S (1985) Production of CO and CH_4 in electrochemical reduction of CO_2 at metal electrodes in aqueous hydrogencarbonate solution. *Chem Lett* 14:1695–1698.
3. Hori Y, Wakebe H, Tsukamoto T, Koga O (1994) Electrocatalytic process of CO selectivity in electrochemical reduction of CO_2 at metal electrodes in aqueous media. *Electrochim Acta* 39:1833–1839.
4. Hori Y (2008) Electrochemical CO_2 reduction on metal electrodes. *Modern Aspects of Electrochemistry*, eds Vayenas C, White R, Gamboa-Aldeco M (Springer, New York) Vol 42, pp 89–189.
5. Gattrell M, Gupta N, Co A (2006) A review of the aqueous electrochemical reduction of CO_2 to hydrocarbons at copper. *J Electroanal Chem* 594:1–19.
6. Kuhl KP, Cave ER, Abram DN, Jaramillo TF (2012) New insights into the electrochemical reduction of carbon dioxide on metallic copper surfaces. *Energy Environ Sci* 5:7050–7059.
7. Kuhl KP, et al. (2014) Electrocatalytic conversion of carbon dioxide to methane and methanol on transition metal surfaces. *J Am Chem Soc* 136:14107–14113.
8. Kim YG, Javier A, Baricuatro JH, Soriaga MP (2016) Regulating the product distribution of CO reduction by the atomic-level structural modification of the cu electrode surface. *Electrocatalysis* 7:391–399.
9. Roberts FS, Kuhl KP, Nilsson A (2015) High selectivity for ethylene from carbon dioxide reduction over copper nanocube electrocatalysts. *Angew Chem Int Ed* 54:5179–5182.
10. Loiudice A, et al. (2016) Tailoring copper nanocrystals towards C_2 products in electrochemical CO_2 reduction. *Angew Chem Int Ed* 55:5789–5792.
11. Ma M, Djanashvili K, Smith WA (2016) Controllable hydrocarbon formation from the electrochemical reduction of CO_2 over cu nanowire arrays. *Angew Chem Int Ed* 55:6680–6684.
12. Li CW, Kanan MW (2012) CO_2 reduction at low overpotential on cu electrodes resulting from the reduction of thick Cu_2O films. *J Am Chem Soc* 134:7231–7234.
13. Kas R, et al. (2014) Electrochemical CO_2 reduction on Cu_2O-derived copper nanoparticles: Controlling the catalytic selectivity of hydrocarbons. *Phys Chem Chem Phys* 16:12194–12201.
14. Li CW, Ciston J, Kanan MW (2014) Electroreduction of carbon monoxide to liquid fuel on oxide-derived nanocrystalline copper. *Nature* 508:504–507.
15. Mistry H, et al. (2016) Highly selective plasma-activated copper catalysts for carbon dioxide reduction to ethylene. *Nat Commun* 7:12123.
16. Dutta A, Rahaman M, Luedi NC, Mohos M, Broekmann P (2016) Morphology matters: Tuning the product distribution of CO_2 electroreduction on oxide-derived cu foam catalysts. *ACS Catal* 6:3804–3814.
17. Xiao H, Cheng T, Goddard WA, Sundararaman R (2016) Mechanistic explanation of the pH dependence and onset potentials for hydrocarbon products from electrochemical reduction of CO on Cu(111). *J Am Chem Soc* 138:483–486.
18. Xiao H, Cheng T, Goddard WA (2017) Atomistic mechanisms underlying selectivities in C_1 and C_2 products from electrochemical reduction of CO on Cu(111). *J Am Chem Soc* 139:130–136.
19. Sundararaman R, Goddard WA (2015) The charge-asymmetric nonlocally determined local-electric (CANDLE) solvation model. *J Chem Phys* 142:064107.
20. Petrosyan SA, Rigos AA, Arias TA (2005) Joint density-functional theory: *Ab initio* study of Cr_2O_3 surface chemistry in solution. *J Phys Chem B* 109:15436–15444.
21. Letchworth-Weaver K, Arias TA (2012) Joint density functional theory of the electrode-electrolyte interface: Application to fixed electrode potentials, interfacial capacitances, and potentials of zero charge. *Phys Rev B* 86:075140.
22. Cheng T, Xiao H, Goddard WA (2016) Reaction mechanisms for the electrochemical reduction of CO_2 to CO and formate on the Cu(100) surface at 298 K from quantum mechanics free energy calculations with explicit water. *J Am Chem Soc* 138:13802–13805.
23. Bendavid LI, Carter EA (2013) CO_2 adsorption on Cu_2O(111): A DFT+U and DFT-D study. *J Phys Chem C* 117:26048–26059.
24. Soon A, Todorova M, Delley B, Stampfl C (2007) Thermodynamic stability and structure of copper oxide surfaces: A first-principles investigation. *Phys Rev B* 75:125420.
25. Önsten A, Göthelid M, Karlsson UO (2009) Atomic structure of Cu_2O(111). *Surf Sci* 603:257–264.
26. Nie X, Griffin GL, Janik MJ, Asthagiri A (2014) Surface phases of Cu_2O(111) under CO_2 electrochemical reduction conditions. *Catal Commun* 52:88–91.
27. Bendavid LI, Carter EA (2013) First-principles predictions of the structure, stability, and photocatalytic potential of Cu_2O surfaces. *J Phys Chem B* 117:15750–15760.
28. Lian X, Xiao P, Yang SC, Liu R, Henkelman G (2016) Calculations of oxide formation on low-index Cu surfaces. *J Chem Phys* 145:044711.
29. Schouten KJP, Qin Z, Gallent EP, Koper MTM (2012) Two pathways for the formation of ethylene in CO reduction on single-crystal copper electrodes. *J Am Chem Soc* 134:9864–9867.
30. Schouten KJP, Pérez Gallent E, Koper MTM (2014) The influence of pH on the reduction of CO and to hydrocarbons on copper electrodes. *J Electroanal Chem* 716:53–57.
31. Gao S, et al. (2016) Partially oxidized atomic cobalt layers for carbon dioxide electroreduction to liquid fuel. *Nature* 529:68–71.
32. Montoya JH, Shi C, Chan K, Nørskov JK (2015) Theoretical insights into a CO dimerization mechanism in CO_2 electroreduction. *J Phys Chem Lett* 6:2032–2037.
33. Nie X, Esopi MR, Janik MJ, Asthagiri A (2013) Selectivity of CO_2 reduction on copper electrodes: The role of the kinetics of elementary steps. *Angew Chem Int Ed* 52:2459–2462.
34. Kresse G, Hafner J (1993) Ab initio molecular dynamics for liquid metals. *Phys Rev B* 47:558–561.
35. Kresse G, Furthmuller J (1996) Efficiency of ab-initio total energy calculations for metals and semiconductors using a plane-wave basis set. *Comput Mater Sci* 6:15–50.
36. Kresse G, Furthmuller J (1996) Efficient iterative schemes for ab initio total-energy calculations using a plane-wave basis set. *Phys Rev B* 54:11169–11186.
37. Perdew JP, Burke K, Ernzerhof M (1996) Generalized gradient approximation made simple. *Phys Rev Lett* 77:3865–3868.
38. Kresse G, Joubert D (1999) From ultrasoft pseudopotentials to the projector augmented-wave method. *Phys Rev B* 59:1758–1775.
39. Henkelman G, Uberuaga BP, Jónsson H (2000) A climbing image nudged elastic band method for finding saddle points and minimum energy paths. *J Chem Phys* 113:9901–9904.
40. Henkelman G, Jónsson H (1999) A dimer method for finding saddle points on high dimensional potential surfaces using only first derivatives. *J Chem Phys* 111:7010–7022.
41. Bertie JE, Whalley E (1967) Optical spectra of orientationally disordered crystals. II. Infrared spectrum of ice Ih and ice Ic from 360 to 50 cm^{-1}. *J Chem Phys* 46:1271–1284.
42. Liu H, Wang Y, Bowman JM (2013) Vibrational analysis of an ice Ih model from 0 to 4000 cm^{-1} using the ab initio WHBB potential energy surface. *J Phys Chem B* 117:10046–10052.
43. Sundararaman R, Gunceler D, Letchworth-Weaver K, Schwarz KA, Arias TA (2012) JDFTx. Available at jdftx.org/. Accessed November 2, 2016.
44. Garrity KF, Bennett JW, Rabe KM, Vanderbilt D (2014) Pseudopotentials for high-throughput DFT calculations. *Comput Mater Sci* 81:446–452.
45. Arias TA, Payne MC, Joannopoulos JD (1992) Ab initio molecular dynamics: Analytically continued energy functionals and insights into iterative solutions. *Phys Rev Lett* 69:1077–1080.
46. Freysoldt C, Boeck S, Neugebauer J (2009) Direct minimization technique for metals in density functional theory. *Phys Rev B* 79:241103.